J. Mater. Chem. A

ARTICLE

Monitoring the Assembly-Disassembly-Organisation-Reassembly Process of Germanosilicate UTL through *in situ* Pair Distribution Function Analysis

Received 00th January 20xx,
Accepted 00th January 20xx

DOI: 10.1039/x0xx00000x

www.rsc.org/

Susan E. Henkelis,[a] Samuel A. Morris,[a,b] Michal Mazur,[a,c] Paul S. Wheatley,[a] Lauren N. McHugh[a] and Russell E. Morris[a,c*]

A study into the disassembly and organisation steps of the ADOR process has been undertaken through *in situ* Pair Distribution Function (PDF) analysis. Three aqueous systems (water, 6 M HCl and 12 M HCl) were introduced to a parent zeolite germanosilicate **UTL** in a cell. Hydrolysis could be clearly seen when **UTL** was exposed to water over a period of 8 hr, forming the disorded layered material, IPC-1P. In hydrochloric acid, the hydrolysis step is too quick to observe and a Ge-Cl containing species could be seen. In 6 M HCl, the rearrangement of the interlayer region began after an induction period of 8 hr, with the process still occuring after 15 hr. In 12 M HCl, the rearrangement appears to have come to an end after only 6 hr.

Introduction

Zeolites or zeotypes can be classed as inorganic crystalline materials with a regular pore network that comprise TO_4 tetrahedra (where T can be Al, B, Ge, P, Si, Ti, etc.).[1–3] Zeolites are typically formed through solvothermal conditions in the presence of a structure-directing agent (SDA).[4,5] An alternative synthetic route to make new zeolites has been created, coined the Assembly, Disassembly, Organisation, and Reassembly (ADOR) process.[1,6–8] The ADOR process takes a pre-assembled parent germanosilicate (for example **IWR**,[7] **IWW**,[6] SAZ-1,[9] **UOV**,[10,11] or **UTL**[12,13]) and selectively breaks it apart in a controlled manner by exploiting the chemical weakness present in germanium-containing building units.[1,14,15] Parent zeolites selected for the ADOR process contain double-four-ring (d4r) units that are preferentially occupied by germanium.[6,7] These Ge-rich d4r can then be hydrolysed into solution by water or aqueous hydrochloric acid to leave behind silica-rich 2D layers, which can in turn be organised into a suitable orientation through the use of an SDA.[8] Upon calcination, the silanol groups on the surface of opposing layers condense to form new daughter zeolites. Many of these daughter zeolites cannot be prepared through traditional methods, and therefore are thought of as 'unfeasible'.[8]

As the ADOR mechanism proceeds, some crystallographic order is lost as the 2D layers are formed. This makes traditional diffraction methods unsuitable for studying the process *in situ*. However, Pair Distribution Function (PDF) analysis proves to be useful in probing these disordered structures as the technique does not rely on crystallographic order.

The Pair Distribution Function (PDF), G(*r*), is the distribution of density of interatomic distances in a given material.[16,17] The PDF can be obtained directly from high energy X-ray or neutron diffraction data by a Fourier transform of the scattering intensity data.[18–20] The main advantage of this technique is that while traditional diffraction methods only use Bragg scattering, PDF analysis is a total scattering method that treats both the sharp Bragg peaks and the broad diffuse scattering equally, thus allowing one to probe both amorphous and crystalline materials on short- or long-range order.[20,21] Historically, this technique has been used to characterise the structures of liquids and glasses, but has since been used for fully or semi-crystalline materials such as metal-organic frameworks[22,23] and zeolites.[24–26]

Analysis through PDF has become increasingly used due to the improved availability of instruments and user-friendly software.[27–30] PDF allows for structure changes in both solid – solid transformations and crystallization of solids to be monitored *in situ*.[21,31–33] Analysis of zeolites and silicates through *in situ* PDF allow for a more thorough examination of both the nucleation and crystal transformations over time or due to a temperature change.[27,34–38] The success of recent *in situ* total scattering experiments can be attributed to dedicated beamlines with large area detectors allowing for high *q*-measurements in a short time.

Understanding the mechanisms of creation and modifications of zeolites is still not complete. Herein, we present the detailed insight into the mechanism of hydrolysis of germanosilicates,

[a] School of Chemistry, EaStChem, University of St. Andrews, North Haugh, St. Andrews, Fife, KY16 9ST, United Kingdom.
[b] Faculty for Analysis, Characterization, Testing and Simulation, Nanyang Technological University, 50 Nanyang Avenue, 639798, Singapore.
[c] Department of Physical and Macromolecular Chemistry Faculty of Sciences, Charles University Hlavova 8, 128 43 Prague 2, Czech Republic

Fig. 1. A schematic representation of the ADOR process from parent germanosilicate **UTL**. Step 1 proceeds through the fast hydrolysis in water to form the disordered IPC-1P layers. Upon treatment with hydrochloric acid these layers begin to rearrange themselves (step 2). Finally, in step 3, the rearrangement is coming to an end and the new daughter zeolite is beginning to be formed. Upon calcination IPC-2 (shown here) would be afforded. The rate of the final two steps are greatly increased by an increase in molarity of acid, [H^+].

showing the great potential of the *in situ* PDF method. It has shown that PDF can be of great support and complementary to X-ray diffraction and solid-state NMR spectroscopy for the mechanism description. The hydrolysis of Ge-**UTL** is relatively easy (in comparison to more complicated processes, like solvothermal synthesis) to reveal using *in situ* PDF when supported by other techniques. This is a step towards the better understanding of the ADOR mechanism, hence making it more useful for more complicated tasks such as precise description of the zeolite crystallisation process.

Here we present *in situ* PDF data to monitor the hydrolysis (Disassembly) and rearrangement (Organisation) mechanisms in the ADOR process in three aqueous systems (water, 6 M aq. HCl, and 12 M aq. HCl). This work showcases the selectivity of the ADOR process in different media and the mechanism by which the d4r breakdown in **UTL** occurs.

Materials and Methods

Synthesis of Parent Ge-UTL with molar composition 0.8 SiO_2: 0.4 GeO_2: 0.4 ROH: 30 H_2O. Germanium dioxide (1.08 g) was dissolved in (6R, 10S)-6,10-dimethyl-5 azoniaspiro, [4,5]decane hydroxide (15 mL, 0.625 M).[39] Fumed silicon dioxide (1.25 g) was added portion-wise to the mixture over 30 mins until a homogeneous solution was formed. The gel was transferred to a Teflon-lined autoclave and heated at 175 °C for 10 days. The zeolite product was collected by filtration, washed with water (200 mL) and dried at 70 °C for 12 hr. To remove the SDA, the as-synthesized zeolite was calcined in a stream of air at 575 °C for 7 hr with a temperature ramp of 1 °C min^{-1}.

Characterisation Techniques

Lab X-ray Diffraction. Lab powder X-ray diffraction data (PXRD) were collected on both a Panalytical Empyrean diffractometer monochromated with a curved Ge(111) crystal in reflectance mode, and a STOE STADIP operated in capillary Debye-Scherrer mode, both diffractometers operating Cu $K_{\alpha 1}$ radiation.

PDF Measurements. PDF measurements were performed at beamline I15 at Diamond Light Source using a custom-made liquid cell adapted for X-ray transmission.[40] Measurements were taken using an X-ray beam of energy 72 keV (λ = 0.1722 Å) and an amorphous silicon area detector (PerkinElmer). Data were collected at 300 s intervals, using a total exposure time of 10 s per scan. For all PDF and XRD experiments, background measurements were taken using the cell, but without the sample present. A CeO_2 standard was used to determine the sample-to-detector distance.

A brass environmental cell was used to monitor the hydrolysis (disassembly) and rearrangement (organisation) steps in the ADOR process. The cell walls were made up of a spacer, Kapton windows, Viton and PTFE washers, a piston and a screw, which form an internal void with a diameter of 13 mm with a depth of 3 mm.[40]

Water, 6 M HCl and 12 M HCl (0.5, 0.6, and 0.6 mL, respectively) were added slowly to calcined **UTL** (120, 80, and 50 mg, respectively) to make a slurry within the cell. Differing amounts of **UTL** were used for each reaction, as the level of viscosity changed dramatically when hydrochloric acid was used. Due to this more **UTL** was needed to make a slurry within the cell for the reaction run in water. The cell was then placed in a heating mantle with three thermocouples attached. The heating mantle was set 10 °C above the required temperature to maintain a temperature gradient over the whole cell window (50, 100, and 100 °C). The cell used could not accommodate agitation or stirring and as such the *in situ* PDF data collected may not be quantitative, but the work does reveal implicit qualitative trends that are useful in determining how the ADOR process proceeds.

PDF Analysis. The PDF, *G(r)*, was obtained through a Fourier transformation of the total scattering function, *S(Q)* (Eq. 1).

$$G(r) = \frac{2}{\pi} \int_{Q_{min}}^{Q_{max}} Q[S(Q) - 1] \sin(Qr)\, dQ \qquad (1)$$

Where the momentum transfer, *Q* can be defined as (Eq. 2):

$$Q = \frac{4\pi \sin\theta}{\lambda} \qquad (2)$$

The PDF data were obtained using PDFgetX2 [41] and the *G(r)* further analysed by a real space Rietveld-type refinement in the PDFgui software package.[42] The refinement parameter R_{cut} was set at 3.38 Å, the maximum distance where correlated motion still has an effect on the material. All fits had a lower limit of 1.38 Å, peaks found below here do not have any physical meaning as heavy atom contacts shorter than this distance are not possible for these materials. Such peaks can be attributed to experimental and Fourier termination errors.

Results and Discussion

Figure 1, shows a representation of the ADOR process as it currently stands. This has been determined through *ex situ* experiments (XRD,[9,43] NMR,[9,44] and PDF[15]) together with *in situ* NMR and XRD on certain parts of the process.[45] It shows the initial hydrolysis of the parent **UTL** and deintercalation of the germanium, silicon and oxygen atoms that make up the interlayer d4r units. Once all the atoms have been removed from the interlayer space the partially ordered IPC-1P is formed.[1] As the mechanism proceeds the IPC-1P becomes more ordered (as evidenced by decreasing full-width-half-max of the diffraction lines in XRD studies). Eventually, under certain conditions, a reintercalation and reorganisation process occurs where silicon (but not germanium) is reintroduced into the interlayer space, eventually connecting the layers together and forming a new precursor zeolite, which we call IPC-2P. Calcination at > 550 °C in air leads to condensation of the majority of any remaining unconnected silanol groups condensing and the formation of the fully connected zeolites IPC-4 and IPC-2 from IPC-1P and IPC-2P respectively. Other materials can be prepared by controlling the relative orientation of the layers prior to calcination.[8,31,46] The rate of the final two steps are greatly enhanced by an increase in hydrochloric acid concentration, [H^+] (Fig. 1).

A very convenient method for following the progress of the disassembly and organisation steps of the ADOR process *ex situ* is X-ray diffraction. Samples of solid can be removed from the reaction as it progresses, and the change in scattering angle (2θ) for the 200 reflection in the XRD, which essentially measures the interlayer d-spacing, can be plotted. Such plots demonstrate how the 200 peak moves quickly to higher values (shorter interlayer spacing) as IPC-1P is formed, before moving to lower values as IPC-2P is formed (Fig. 2).

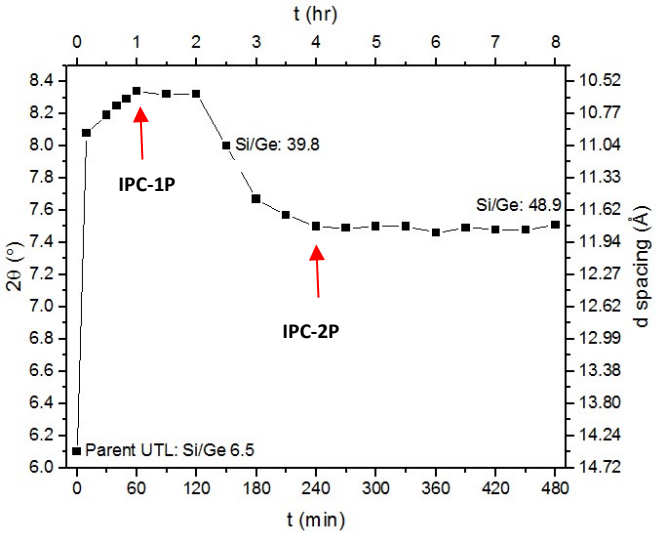

Fig. 2. Plot of the measured scattering angle (2θ) of the 200 peak versus time as the ADOR process proceeds on hydrolysis of UTL in water at 100 °C. The X-ray powder diffraction data is collected ex situ after recovery of a portion of the sample from the reaction mixture. The layered structure IPC-1P is formed at 1 hr (indicated by a 2θ of ~8.3°, before finally rearranging to IPC-2P after around 4 hours (2θ ~7.5°)

In situ total scattering experiments were completed on beamline I15 at the Diamond Light Source, UK. The Bragg reflections in the experiment for **UTL** in water show a sharpening of the 200 peak and a shift to slightly increased 2θ, giving a change in d-spacing from 14.10 to 13.74 Å (as-synthesized **UTL** – 14.49 Å). This change has also been seen in lab-based *ex situ* studies, where upon hydrolysis with water, the Si-O-Ge or Ge-O-Ge bonds preferentially located within the Ge-rich d4r are broken and the resulting species removed from the interlayer space. The Si-O-Si bonds located within the layers are largely unaffected leaving the IPC-1P structure.

There is a clear increase in reactivity for the *in situ* reactions undertaken in acid. This occurrence has also been noted in *ex situ* studies for the formation of IPC-6 and IPC-2, where a high concentration of HCl is also used.[45] Moreover, the low volume *in situ* process is visibly slower than the *ex situ* hydrolysis in high volume.

Pair Distribution Function Analysis

UTL in Water

The pair distribution function, $\boldsymbol{G(r)}$ was plotted for **UTL** in water over a period of 8 hr (Fig. 3; E.S.I Fig. 3a-b for long r-range data). The initial Ge-**UTL** PDF shows broad T-O and T-T peaks because there are both Si and Ge contributing to the peaks. The initial disassembly process occurs quickly, but we are still able to see some evidence of germanium in the materials as we can see clear shoulders at longer distance on both the T-O and T-T peaks

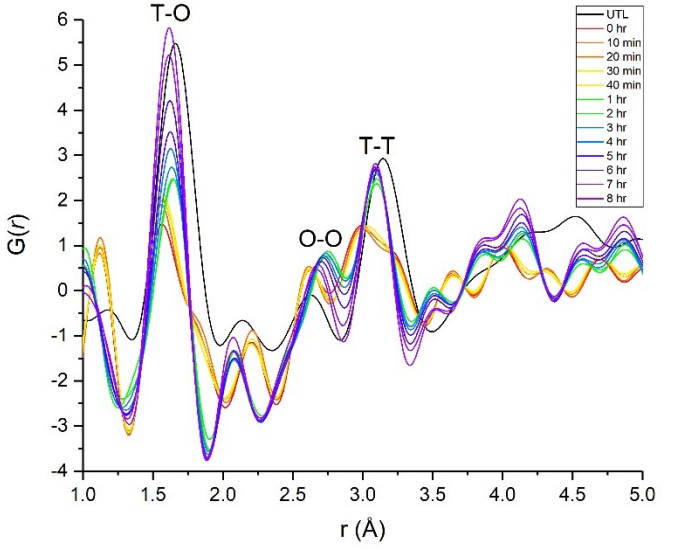

Fig. 3. Experimental Pair Distribution Function data for the hydrolysis of **UTL** treated in water over a timeframe of 8 hr at 100 °C, with hydrolysis information shown every 10 min for the first hr and every hour thereafter.

in Figure 3 (the regions showing this best are shown in orange shades in the PDFs). Once all the Ge has been removed we are then left with only Si contributing to the peaks. These are therefore much sharper than in the parent Ge-**UTL**. At this point the layered IPC-1P is formed and organises itself fairly quickly into the final PDF, with peak positions that remain broadly unchanged over the remainder of the experiment (this region is shown in purple/green shades in Figure 3)

Over this timeframe we can also see changes in the PDF intensities with the peak representing the T-O (1.62 Å; where T = Si, Ge) distances increasing in intensity over time. This is as expected as when hydrolysis occurs, T-O-T linkages are broken down, with an additional oxygen atom added over the linkage, therefore giving rise to two T-O pairs with more atoms (and therefore electrons) contributing to the scattering, and as such we see an increase in the T-O peak in the PDF histogram.

To confirm these results, the *ex situ* PXRD patterns of the recovered products of **UTL** after hydrolysis and rearrangement was measured over a period of 8 hr (See Fig. 2). An increase in the scattering angle of the 200 diffraction peak (the diffraction peak that gives the interlayer distance in the material) gives clear indication of the breakdown of the d4r (up to 1 hr), forming the disordered layered structure, IPC-1P, before the rearrangement to IPC-2P after an induction period of ~1 hr.

The structure then stabilises at this product after 3 hr. The conditions of this experiment are not exactly analogous to the PDF work because of experimental restrictions, but does confirm that the processes seen *in situ* are broadly the same as those that can be inferred *ex situ* after product recovery.

The area under the curve for the three most notable peaks, T-oxygen (T-O, 1.62 Å), oxygen-oxygen (O-O, 2.69 Å) and T-T (3.11 Å), in the PDF were plotted as a function of time (Fig. 4). It is

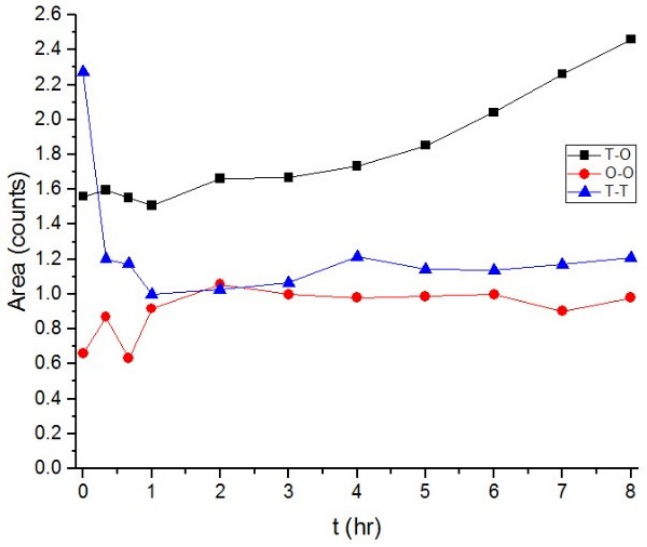

Fig. 4. Area under the curve for **UTL** treated in water over 8 hr for peaks in the PDF that can be identified as arising from T-O, O-O and T-T interatomic pairs.

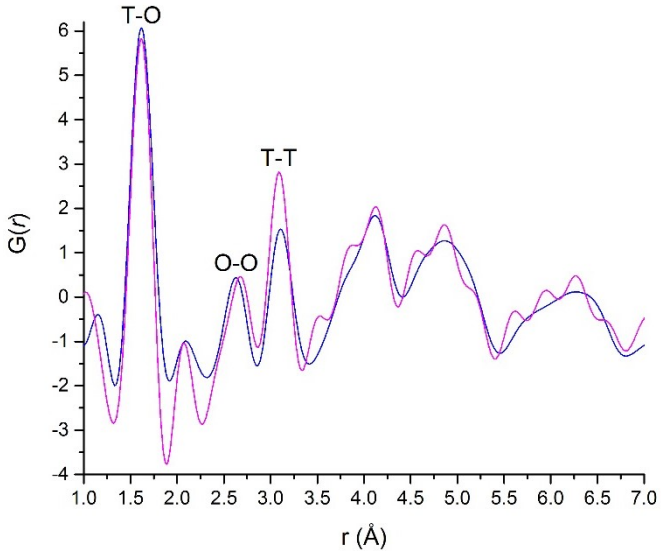

Fig. 5. Comparison of experimentally derived PDF data for *in situ* **UTL** treated in water at 100 °C (pink) vs. *ex situ* IPC-1P that has been isolated and recovered (blue).

noteworthy to say that the peaks for each shift over time and therefore, the distances given above are an average. A significant increase in the T-O peak can be seen, corroborating with the results from the intensity of the PXRD d-spacing that the germanium rich d4r have broken down by hydrolysis and the silanol groups that remain in the 2D layers are now coming closer together over time. Again, this change in area follows the same trend as both total scattering *in situ* PDF and the *ex situ* Bragg scattering data.

The final *in situ* run was plotted against an existing ADORable daughter zeolite in its hydrolysed state before calcination, specifically IPC-1P (collected *ex situ*; Fig. 5). IPC-1P is a suitable candidate for comparison as it is formed chemically through the same conditions.[1] From the comparison we can see great similarity between each PDF with only minor discrepancies between the two.

To fully confirm our results, a Rietveld-type refinement of an IPC-1P model against the experimental PDF data was undertaken and its structure obtained (Fig. 6). It is clear that IPC-1P has been formed, however due to the PDF produced *in situ*, there are free water and germanium oxide/hydroxide species (e.g. the peak at 3.47 Å) present that are not modelled and this leads to a fit with a R_w of only 38%. However, from the PXRD, experimental PDF data and the refinement it is clear that we have formed the highly disordered material IPC-1P, and followed the hydrolysis of the d4r within **UTL**.

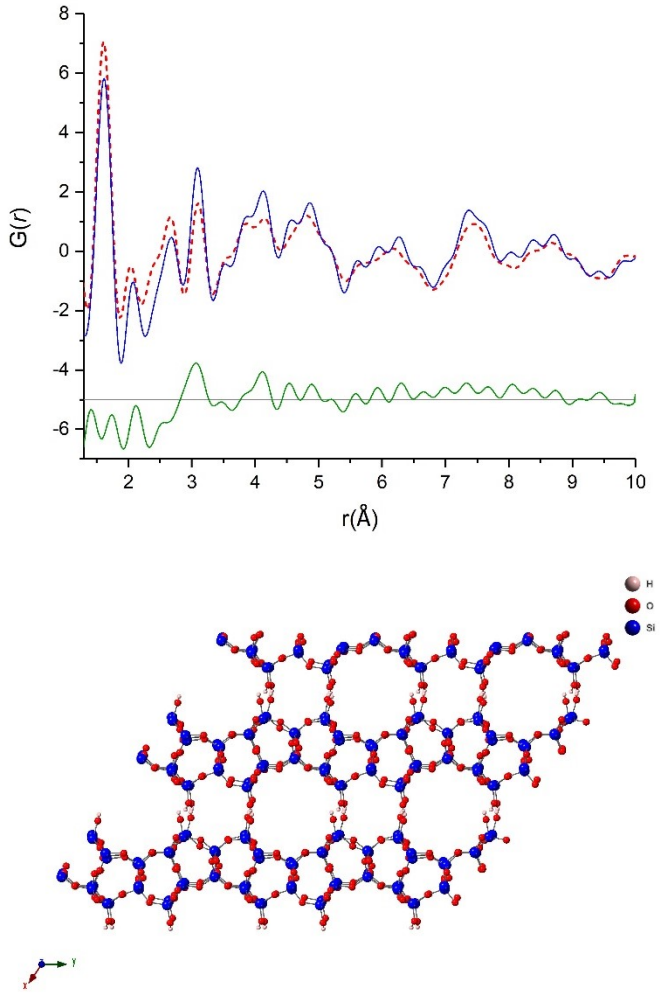

Fig. 6. TOP: Refinement of the IPC-1P model against in situ PDF data. R_w = 38%. The blue solid line is experimental data, the red dashed line is the calculated PDF from the model and the green line is the difference between the two, offset by -5. Bottom: The PDF refinement of IPC-1P viewed across the c-axis. Si – blue; O – red; H – pink.

UTL in 6 M Hydrochloric Acid

The X-ray scattering data was processed and a Fourier transform performed to formulate the PDF for **UTL** in 6 M HCl over a period of 15 hr. Owing to the fairly high HCl concentration, a peak due to a germanium-chloride (Ge-Cl) species can now be seen at 2.08 Å (Fig. 7), together with another extra peak at ~3.5 Å, which likely corresponds to next nearest neighbour Ge-Ge species. Such features have not been seen before in our previous *ex situ* studies. The presence of a Ge-Cl peak that grows with time allows for a better insight into the mechanism of the ADOR process, specifically the disassembly and organisation steps. It shows us that the germanium is not only hydrolysed by the water content in the aqueous acid, but that high [H^+] and [Cl^-] rapidly speeds up that process and plays

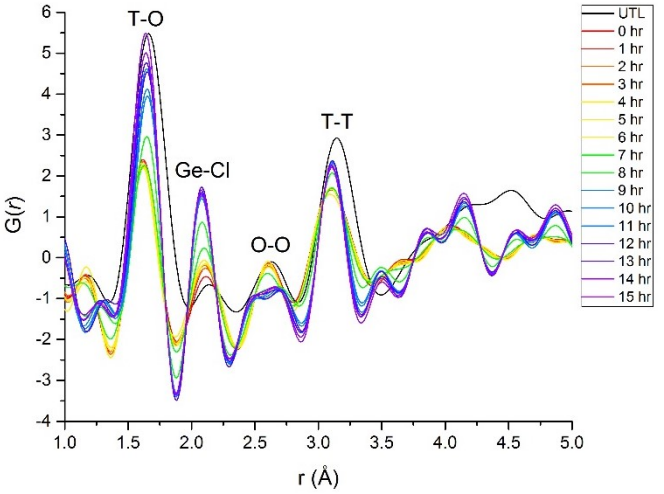

Fig. 7. Experimental Pair Distribution Function data for the rearrangement of **UTL** treated in 6 M HCl over a timeframe of 15 hr at 100 °C vs. parent UTL.

a special role in the disassembly mechanism by attacking the d4r.

The initial hydrolysis step, which was observed in water, is now over too quickly to be measured. Little change is seen up to 8 hr, from then on both the T-O and Ge-Cl peaks increase. This fits with the hypothesis that after the hydrolysis there is an induction period before the system shows reintercalation of silicon species from the solution and rearrangement occurs.

This rearrangement of the layers then begins to occur after approximately 8 hr. The area under each peak were once again recorded and plotted as a function of time, the induction period upto 8 hr can be seen with the rearrangement occuring from 8 up to 15 hr (Fig 8).

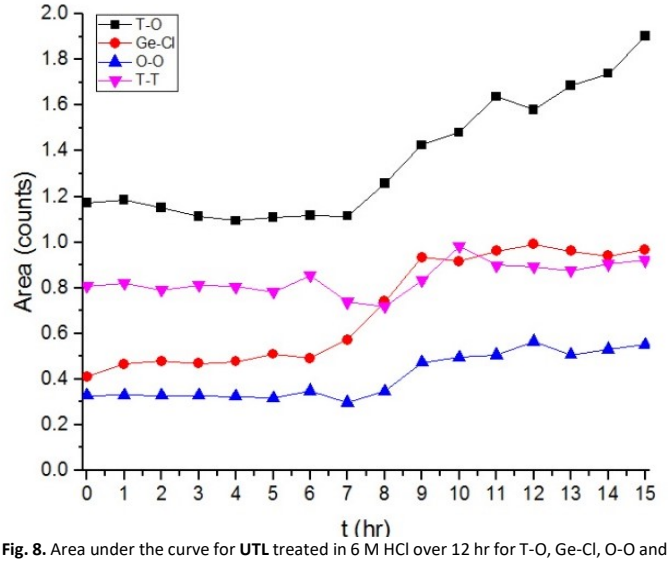

Fig. 8. Area under the curve for **UTL** treated in 6 M HCl over 12 hr for T-O, Ge-Cl, O-O and T-T interatomic pairs.

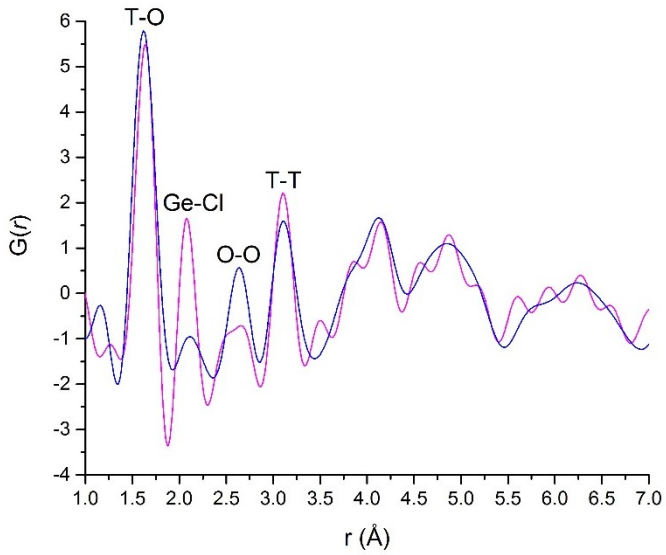

Fig. 9. PDF comparison of *in situ* **UTL** treated in 6 M HCl at 100 °C (pink) vs. IPC-7P prepared *ex situ* (blue).

The final *in situ* run at 15 hr of treated **UTL** in 6 M HCl was compared with a synthetic IPC-7P (Fig. 9). IPC-7P is made from parent zeolite **UTL**, via disassembly into IPC-1P and then rearrangement into IPC-7P.[46] IPC-7P has some rearranged silicon in between the layers, and upon calcination would form IPC-7, containing layers of s4r and d4r. Disregarding the Ge-Cl species at 2.08 Å (Ideal Ge-Cl = 2.1 Å) and the peak at about 3.5 Å [47] which would not be present in any *ex situ* measurement of zeolites, it can be said that there are similarities between the PDFs.

The T-O and T-T peaks are largely the same, however the significant change in the O-O peak tells us that IPC-7P has not been fully formed. Moreover, the rearrangement process may not have come to an end. The experiment time is limited due to drying of the system, however it can be said that with more reaction time the final product would be IPC-7P.

UTL in 12 M Hydrochloric Acid

Finally, a slurry of **UTL** in 12 M HCl was prepared and over 12 hr a clear change can be seen when the PDF is compared to parent **UTL**. Again, the hydrolysis step is missed. However, unlike 6 M HCl, the reaction seems to be almost completed and no induction period can be seen between the hydrolysis and rearrangement processes (Figs. 10 and 11).

UTL in 12 M HCl was compared against an *ex situ* collected PDF of IPC-2P which is formed through conditions of 95 °C and 12 M HCl (Fig. 12). Again extra peaks at 2.1 Å and 3.47 Å can be seen, due to Ge-Cl and next nearest neighbour Ge-Ge internuclear distances produced from the formation of Ge-containing species during hydrolysis of the d4r.[48]

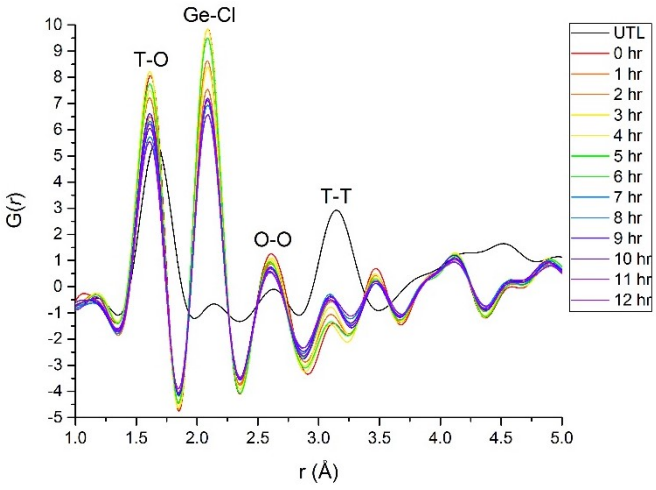

Fig. 10. Experimental Pair Distribution Function data for the rearrangement of **UTL** treated in 12 M HCl over a timeframe of 12 hr at 50 °C vs. parent **UTL**.

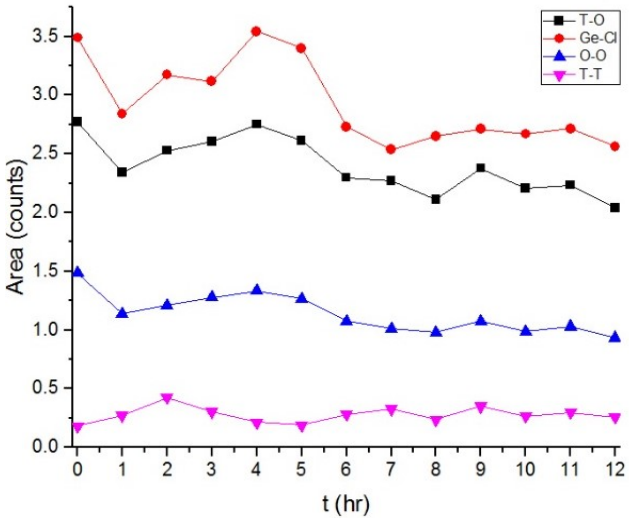

Fig. 11. Area under the curve for **UTL** treated in 12 M HCl over 12 hr for T-O, Ge-Cl, O-O and T-T interatomic pairs.

Mechanism

There is data in all three *in situ* PDF spectral series beyond 10 Å (and even out to significantly longer distances, see supplementary information). This agrees well with the proposed mechanism of the process as shown in Figure 1. Because of the selective siting of the germanium atoms in the d4r units that lie between the silica-rich layers, the hydrolysis process has little or no effect on the basic structure of the layers themselves. Therefore, the ADOR process keeps the order in the 2D layers almost intact throughout the process. This is the first time this has been seen in an *in situ* experiment, and answers one of the most often questions asked about the ADOR process:

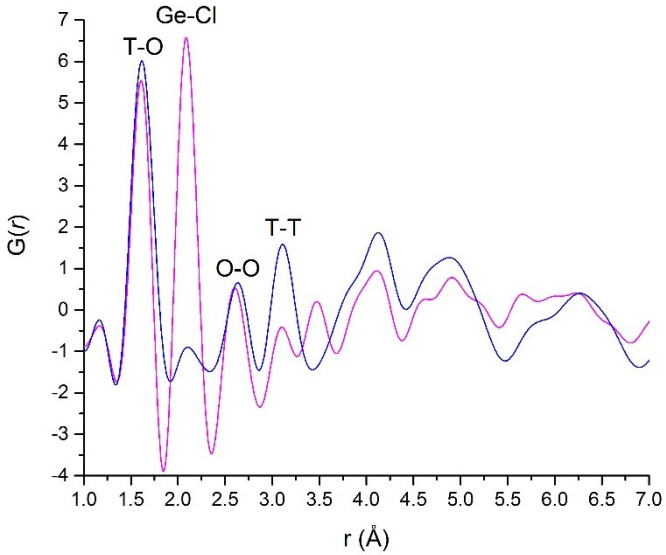

Fig. 12. PDF comparison of in situ **UTL** treated in 12 M HCl at 50 °C (pink) vs. IPC-2P prepared *ex situ* (blue).

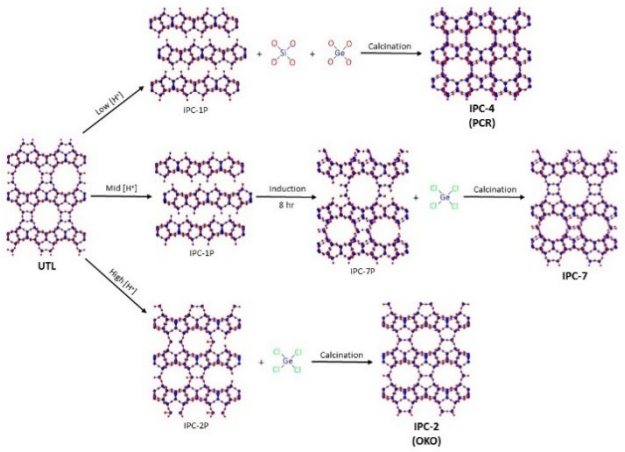

Fig. 13. The detailed reaction scheme as revealed by in situ PDF studies

could the final products be explained by a dissolution/recrystallization mechanism. The *in situ* studies presented here show that the mechanism does not occur via such a route. Therefore, the fact that we have been able to follow the process of the reaction *in situ* yields important results that are not available by other means.

While the order within the layers is retained, the interlayer order is lost during the disassembly step of the process, during the organisation steps in the presence of acid some silicon species reintercalate in between the layers. Simultaneously, this orders the layers somewhat by linking them together, but at the same time also introduces further disorder as the intercalation does not happen in any ordered manner. The region beyond about 5 Å is complex, and it is particularly difficult to assign direct structural features to due to the large number of similar-sized ring structures causing a large amount of overlap between nearest neighbours.[15] Future work will involve using multi-technique studies to identify the nature of the interlayer species with more accuracy.

The three different *in situ* X-ray PDF experiments reported in this paper give some important new insights into the ADOR process. Although missing the very initial hydrolysis for two of the reactions we have, for the first time, been able to follow the process *in situ,* through use of different aqueous media (previous work using NMR and XRD only enabled certain parts of the process to be followed). The overall conclusions from the study can be seen in Fig 13. Under low acidity conditions hydrolysis to IPC-1P occurs, with loss of Ge and Si from the system. The PDF of IPC-1P *in situ* is similar to that after isolation, which indicates that there is little change of the material on recovery and drying. This material can be calcined to form the zeolite IPC-4. In 6 M HCl, the hydrolysis produces a species that contains Ge-Cl bonds upon hydrolysis, and there is an induction period before the organisation process occurs. The initial hydrolysis is too fast under these conditions to see. In 12 M HCl the complete process is too fast to observe using the current experimental setup, and no IPC-1P intermediate can be observed.

Conclusions

This is this the first *in situ* study to monitor the disassembly and organisation/rearrangement steps within the ADOR process for parent germanosilicate **UTL**. This mechanistic study shows the slow hydrolysis step when **UTL** is run in water over a period of 8 hr. The breakdown of the germanium rich d4r from between the silica rich layers of **UTL** forms the highly disordered layered material, IPC-1P. In hydrochloric acid, the hydrolysis step has occurred before we were able to record any X-ray data and a Ge-Cl species is now present allowing a deeper insight into the ADOR process. In 6 M HCl, there is an induction period up to 8 hr, before the rearrangement of the layers occurs. The process still seems to be occurring up to 15 hr, whereas in 12 M HCl, the rearrangement process appears to be coming to an end after only 6 hr, thus showing that with an increase of $[H^+]$ present in the reaction, the reactivity of the process increases, whilst also changing the structure of the final material. We can see that with 6 M HCl Ge-**UTL** is rearranged to IPC-7P, and with increase in acid to 12 M, IPC-2P is formed. If these materials were to be calcined, IPC-2 and IPC-7 would be formed, respectively. Future work should contain a more precise study of the ADOR process through *in situ* PDF, by use of a modified cell under flow conditions, which should remove the Ge-containing compounds from the system.

Conflicts of interest

There are no conflicts to declare.

Acknowledgements

The authors would like to thank: The EPSRC (grants: EP/K025112/1; EP/K005499/1; EP/K503162/1) for funding opportunities and beam line I15 at the Diamond Light Source. Phoebe Allan is acknowledged for her help and knowledge of PDF refinement. M.M. and R.E.M. would like to acknowledge OP VVV "Excellent Research Teams", project No. CZ.02.1.01/0.0/0.0/15_003/0000417 - CUCAM.

Notes and references

‡ Large volume *ex situ* synthesis: Ge-**UTL** (600 mg) was added to water (120 mL) with stirring (600 rpm) at 100 °C. Aliquots were taken at 1 min – 30 min intervals for 8 hr. Each sample was filtered under vacuum and dried at 80 °C for 5 min before being packed in 0.5 mm borosilicate capillaries.

1 P. Eliášová, M. Opanasenko, P. S. Wheatley, M. Shamzhy, M. Mazur, P. Nachtigall, W. J. Roth, R. E. Morris and J. Čejka, *Chem. Soc. Rev.*, 2015, **44**, 7177–206.

2 D. W. Breck, *J. Chem. Educ.*, 1964, **41**, 678.

3 C. Baerlocher, L. B. McCusker, D. Olson, W. M. (Walter M. . Meier and International Zeolite Association. Structure Commission., *Atlas of zeolite framework types*, Published on behalf of the Structure Commission of the International Zeolite Association by Elsevier, 2007.

4 C. S. Cundy and P. A. Cox, *Chem. Rev.*, 2003, **103**, 663–701.

5 M. E. Davis and R. F. Lobo, *Chem. Mater*, 1992, **4**, 156–768.

6 P. Chlubná-Eliášová, Y. Tian, A. B. Pinar, M. Kubů, J. Čejka and R. E. Morris, *Angew. Chemie*, 2014, **126**, 7168–7172.

7 M. Shamzhy, M. Opanasenko, Y. Tian, K. Konysheva, O. Shvets, R. E. Morris and J. Čejka, *Chem. Mater.*, 2014, **26**, 5789–5798.

8 M. Mazur, P. S. Wheatley, M. Navarro, W. J. Roth, M. Položij, A. Mayoral, P. Eliášová, P. Nachtigall, J. Čejka and R. E. Morris, *Nat. Chem.*, 2015, **8**, 58–62.

9 D. S. Firth, S. A. Morris, P. S. Wheatley, S. E. Russell, A. M. Z. Slawin, D. M. Dawson, A. Mayoral, M. Opanasenko, M. Položij, J. Čejka, P. Nachtigall and R. E. Morris, *Chem. Mater.*, 2017, **29**, 5605–5611.

10 V. Kasneryk, M. Shamzhy, M. Opanasenko, P. S. Wheatley, S. A. Morris, S. E. Russell, A. Mayoral, M. Trachta, J. Čejka and R. E. Morris, *Angew. Chemie Int. Ed.*, 2017, **56**, 4324–4327.

11 V. Kasneryk, M. Opanasenko, M. Shamzhy, Z. Musilová, Y. S. Avadhut, M. Hartmann and J. Čejka, *J. Mater. Chem. A*, 2017, **5**, 22576–22587.

12 W. J. Roth, O. V Shvets, M. Shamzhy, P. Chlubná, M. Kubů, P. Nachtigall and J. Čejka, *J. Am. Chem. Soc.*, 2011, **133**, 6130–6133.

13 W. J. Roth, P. Nachtigall, R. E. Morris, P. S. Wheatley, V. R. Seymour, S. E. Ashbrook, P. Chlubná, L. Grajciar, M. Položij, A. Zukal, O. Shvets and J. Čejka, *Nat. Chem.*, 2013, **5**, 628–633.

14 R. E. Morris and J. Čejka, *Nat. Chem.*, 2015, **7**, 381–388.

15 S. A. Morris, P. S. Wheatley, M. Položij, P. Nachtigall, P. Eliášová, J. Čejka, T. C. Lucas, J. A. Hriljac, A. B. Pinar and R. E. Morris, *Dalt. Trans.*, 2016, **45**, 14124–14130.

16 M. M. Martínez-Iñesta and R. F. Lobo, *J. Phys. Chem. B*, 2005, **109**, 9389–9396.

17 M. M. Martínez-Iñesta, I. Peral, T. Proffen and R. F. Lobo, *Microporous Mesoporous Mater.*, 2005, **77**, 55–66.

18 X. Qiu, J. W. Thompson and S. J. L. Billinge, *J. Appl. Crystallogr.*, 2004, **37**, 678–678.

19 International Union of Crystallography., *Journal of applied crystallography.*, Blackwell Pub. on behalf of the International Union of Crystallography.

20 T. Egami and S. J. L. Billinge, *Underneath The Bragg Peaks: Structural Analysis of Complex Materials - Second Edition.*, 2012, vol. 7.

21 K. M. Ø. Jensen, M. Christensen, P. Juhas, C. Tyrsted, E. D. Bøjesen, N. Lock, S. J. L. Billinge and B. B. Iversen, *J. Am. Chem. Soc.*, 2012, **134**, 6785–6792.

22 P. K. Allan, P. S. Wheatley, D. Aldous, M. I. Mohideen, C. Tang, J. A. Hriljac, I. L. Megson, K. W. Chapman, G. De Weireld, S. Vaesen and R. E. Morris, *Dalt. Trans.*, 2012, **41**, 4060.

23 P. K. Allan, K. W. Chapman, P. J. Chupas, J. A. Hriljac, C. L. Renouf, T. C. A. Lucas and R. E. Morris, *Chem. Sci.*, 2012, **3**, 2559.

24 J. E. Readman, P. M. Forster, K. W. Chapman, P. J. Chupas, J. B. Parise and J. A. Hriljac, *Chem. Commun.*, 2009, **0**, 3383.

25 V. V. Narkhede and H. Gies, *Chem. Mater.*, 2009, **21**, 4339–4346.

26 A. M. M. Abeykoon, W. Donner, M. Brunelli, M. Castro-Colin, A. J. Jacobson and S. C. Moss, *J. Am. Chem. Soc.*, 2009, **131**, 13230–13231.

27 M. M. Martínez-Iñesta, I. Peral, T. Proffen and R. F. Lobo, *Microporous Mesoporous Mater.*, 2005, **77**, 55–66.

28 S. J. L. Billinge, *Zeitschrift für Krist. - Cryst. Mater.*, , DOI:10.1524/zkri.219.3.117.29094.

29 A.-C. Dippel, H.-P. Liermann, J. T. Delitz, P. Walter, H.

Schulte-Schrepping, O. H. Seeck and H. Franz, *J. Synchrotron Radiat.*, 2015, **22**, 675–687.

30 P. Juhás, T. Davis, C. L. Farrow and S. J. L. Billinge, *J. Appl. Crystallogr.*, 2013, **46**, 560–566.

31 D. Saha, E. D. Bøjesen, A. H. Mamakhel, M. Bremholm and B. B. Iversen, *ChemNanoMat*, 2017, **3**, 472–478.

32 D. Olds, P. F. Peterson, M. K. Crawford, J. R. Neilson, H.-W. Wang, P. S. Whitfield and K. Page, *J. Appl. Crystallogr.*, 2017, **50**, 1744–1753.

33 N. Garg and C. E. White, *J. Mater. Chem. A*, 2017, **5**, 11794–11804.

34 A. M. M. Abeykoon, W. Donner, M. Brunelli, M. Castro-Colin, A. J. Jacobson and S. C. Moss, *J. Am. Chem. Soc.*, 2009, **131**, 13230–13231.

35 V. V. Narkhede and H. Gies, *Chem. Mater.*, 2009, **21**, 4339–4346.

36 M. P. Attfield, M. Feygenson, J. C. Neuefeind, T. E. Proffen, T. C. A. Lucas and J. A. Hriljac, *RSC Adv.*, 2016, **6**, 19903–19909.

37 E. D. Bøjesen and B. B. Iversen, *CrystEngComm*, 2016, **18**, 8332–8353.

38 G. N. Kalantzopoulos, F. Lundvall, S. Checchia, A. Lind, D. S. Wragg, H. Fjellvåg and B. Arstad, *ChemPhysChem*, 2018, **19**, 519–528.

39 M. E. Davis, *Nature*, 2002, **417**, 813–821.

40 G. Sankar and W. Bras, *Catal. Today*, 2009, **145**, 195–203.

41 X. Qiu, J. W. Thompson and S. J. L. Billinge, *J. Appl. Crystallogr.*, 2004, **37**, 678.

42 C. L. Farrow, P. Juhas, J. W. Liu, D. Bryndin, E. S. Božin, J. Bloch, T. Proffen and S. J. L. Billinge, *J. Phys. Condens. Matter*, 2007, **19**, 335219.

43 M. Mazur, A. Arevalo-Lopez, P. S. Wheatley, G. Bignami, S. E. Ashbrook, Á. Morales-García, P. Nachtigall, P. Attfield, J. Cejka and R. Morris, *J. Mater. Chem. A*, , DOI:10.1039/C7TA09248B.

44 G. P. M. Bignami, D. M. Dawson, V. R. Seymour, P. S. Wheatley, R. E. Morris and S. E. Ashbrook, *J. Am. Chem. Soc.*, 2017, **139**, 5140–5148.

45 S. A. Morris, G. P. M. Bignami, Y. Tian, M. Navarro, D. S. Firth, J. Čejka, P. S. Wheatley, D. M. Dawson, W. A. Slawinski, D. S. Wragg, R. E. Morris and S. E. Ashbrook, *Nat. Chem.*, 2017, 1–7.

46 P. S. Wheatley, P. Chlubná-Eliášová, H. Greer, W. Zhou, V. R. Seymour, D. M. Dawson, S. E. Ashbrook, A. B. Pinar, L. B. McCusker, M. Opanasenko, J. Čejka and R. E. Morris, *Angew. Chemie - Int. Ed.*, 2014, **53**, 13210–13214.

47 J. D. Christian, *J. Chem. Educ.*, 1973, **50**, 176.

48 W. H. Baur and A. A. Khan, *Acta Crystallogr. Sect. B Struct. Crystallogr. Cryst. Chem.*, 1971, **27**, 2133–2139.